Dalton Transactions

Accepted Manuscript

ROYAL SOCIETY OF CHEMISTRY

www.rsc.org/dalton

Journal Name

RSCPublishing

ARTICLE

High Efficient Visible-Light Driven Photocatalyst: Two Dimensional Square-like Bismuth Oxyiodine Nanosheets

Y. Mi, M. Zhou, L.Y. Wen, H.P. Zhao and Y. Lei*

Cite this: DOI: 10.1039/x0xx00000x

Received 00th January 2012,
Accepted 00th January 2012

DOI: 10.1039/x0xx00000x

www.rsc.org/

Two dimensional (2D) square-like bismuth oxyiodine (BiOI) nanosheets with thickness of about 10 nm and exposed {001} facets are obtained by a facile hydrothermal route without any surfactant and special solvent. The photocatalytic performance of as-prepared 2D square-like BiOI nanosheets are evaluated by the photodegradation of rhodamine-B (RhB), methyl orange (MO) and phenol under visible-light irradiation. The products show highly efficient photocatalytic performance and good photostability and recyclability under the visible light irradiation. The efficient visible-light driven photocatalytic activity can be ascribed to the thin 2D square shape nanosheet with exposed {001} facet, which provides appropriate diffusion length and self-induced internal static electric fields direction of BiOI, improves the separation efficiency of photoinduced electron-hole pairs in BiOI nanosheets. Furthermore, the thin nanosheets have more percentage of {001} facet exposure could induce stronger internal static electric fields, improve the photocatalytic activity.

1. Introduction

Since the discovery of photocatalytic splitting of water on TiO_2 electrodes in 1972 by Honda and Fujishma,[1] efficient utilization of solar energy for photocatalysis towards environmental purification and solar energy conversion have been attracting massive research interests.[2-3] Various photocatalysts have been prepared and used in photocatalytic water splitting and photodegradation of organic pollutants.[4-10] However, the photocatalysis of many photocatalysts are limited only under ultraviolet irradiation ($\lambda < 380$ nm). Therefore, it is still of great significance to develop visible-light driven photocatalysts for highly efficient solar utilization.

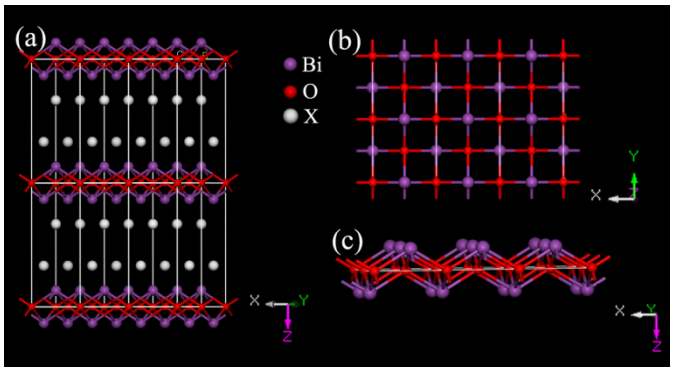

Fig. 1 Schematic representation of the crystal structure of BiOX: (a) Crystal structure of BiOX; (b) {001} facet of BiOX; and (c) $[Bi_2O_2]^{2+}$ layers of BiOX.

Recently, as a series of novel layered ternary oxide semiconductors, bismuth oxyhalides (BiOX, X = Cl, Br, and I) have received much attention because of their excellent photocatalytic performances.[11-18] Bismuth oxyhalides possess a layered structure (as shown in Fig. 1), which is consisting of $[Bi_2O_2]^{2+}$ slabs separated by double slabs of halogen atoms. The space of layered structures is large enough to increase for polarizing the related atoms and orbitals. The induced dipole could then improve the separation efficiency of hole-electron pairs. With the benefits from their open and layered crystalline structures, the bismuth oxyhalides show outstanding photocatalytic performances. BiOCl shows better photocatalytic activity than TiO_2 under ultraviolet irradiation. Furthermore, bismuth oxyhalides can extend light absorption to visible light range. It is highly important for the direct use of sunlight.

As known, properties of materials are determined by their crystalline structures. Meanwhile, the morphology structures are also play important roles. Profiting from high specific surface areas and large fraction of uncoordinated surface atoms, quasi-two-dimensional (quasi-2D) materials have attracted high research interests.[12,16,19-21] For photocatalytic applications, the exposed surface atoms of quasi-2D materials could easily escape from a lattice to form vacancies that could have strong advantageous effect to photocatalytic performance.[12] Especially quasi-2D structures of bismuth oxyhalide shall have largely improved photocatalytic performance, which has been partially approved recently by the excellent visible light photoactivity of BiOCl nanosheets.[11-12,16] For even better visible light absorption comparing with BiOCl, various morphologies of BiOI (Eg = 1.77 ~ 1.92 eV) photocatalysts have also been fabricated.[14,22-27]

However, so far quasi-2D nanostructure of BiOI has rarely been realized and reported. Therefore, nowadays, how to achieve quasi-2D nanostructure of BiOI presents a timely research topic within the field of photocatalytic application of BiOX. In this paper, using a cost-effective and environmental friendly hydrothermal process, 2D square-like BiOI nanosheets with a high percentage of exposed {001} facet were achieved. Different from most of conventional hydrothermal processes using surfactants or special solvent that cause high experimental cost, our non-surfactant process and aqueous system is highly desirable for reducing cost. More importantly, these quasi-2D nanosheets show superior visible-light photocatalytic performance, which shall originates from the highly exposed active facets and several-nanometer thickness of the quasi-2D nanosheets. It is found that after only 15 min visible light irradiation, the decolouration ratio of RhB and MO reaches 90 % and 94 %, respectively.

2. Experimental

2.1 Materials

Poly(3,4-ethylenedioxythiophene)-poly(styrenesulfonate) (PEDOT-PSS) is got from Sigma-Aldrich Co. LLC. All others chemicals were of analytical grade purity, obtained from Alfa Aesar GmbH & Co KG., and used as received without further purification.

2.2 Synthesis of 2D square-like BiOI Nanosheets

The 2D square-like BiOI nanosheets were synthesized using a simple hydrothermal process. In a typical synthesis, 0.485 g of $Bi(NO_3)_3{\cdot}5H_2O$ was dissolved in 20 mL of 0.1M HNO_3 solution with vigorous stirring for 20 min. Next, 20 mL of 0.02 M KI solution was dropwise added into the above solution. Then, the pH value was adjusted to 5 by 5 M KOH solution, yielded a uniform light-yellow suspension. After another 20 min of agitation, the mixture was transferred into a 50 mL capacity Teflon-lined stainless steel autoclave, and this autoclave was heated at the temperature of 120°C for 6 h and then cooled to room temperature naturally. The resulting light-yellow solid powder was collected by centrifugation and washed with deionized water several times to remove residual ions. The final products were then dried at 30°C for 4 h for further characterization.

2.3 Synthesis of BiOI microplates:

For the BiOI microplates, 2.425 g of $Bi(NO_3)_3{\cdot}5H_2O$ was dissolved in 20 mL of 0.1 M HNO_3 solution with vigorous stirring for 20 min. Next, 20 mL of 0.1M KI solution was dropwise added into the above solution, yielded a uniform brick-red suspension. After another 20 min of agitation, the mixture was transferred into a 50 mL capacity Teflon-lined stainless steel autoclave, and this autoclave was heated at the temperature of 120°C for 6 h and then cooled to room temperature naturally. The resulting brick-red solid powder was collected by centrifugation and washed with deionized water several times to remove residual ions. The final products were then dried at 30°C for 4 h for further characterization.

2.4 Characterization:

Powder X-ray diffraction patterns (XRD) were recorded on Bruker D8 Advance equipped with graphite monochromatized high-intensity Cu Kα radiation (λ = 1.54178 Å). The scanning electron microscopy (SEM) images were obtained by HITACHI S4800 scanning electron microscope. The transmission electron microscopy (TEM) images were obtained by JEOL JEM-2010F operated at an acceleration voltage of 100kV. High-resolution transmission electron microscopy (HRTEM) and the corresponding selected area electron diffraction (SAED) analyses were got at an acceleration voltage of 200 kV. Room-temperature UV-Vis absorption spectroscopy was carried out on Varian Cary 5000 UV-VIS-NIR spectrophotometer. The Brunauer-Emmett-Teller (BET) surface areas were measured by nitrogen adsorption on ASAP2020M accelerated surface area and porosimetry system.

2.5 Photocatalytic Measurement:

Visible light photocatalytic activities of the as-prepared products were evaluated by examining the photodegradation of RhB, MO and Phenol under visible light irradiation from 300 W Xe lamp with a 420 nm cut-off filter simulating AM1.5 spectrum (Newport solar simulator). Typically, 10 mg of as-prepared product was added into 50 mL of 2.0×10^{-5} M RhB, 50 mL of 2.0×10^{-5} M MO and 50 mL of 2.0×10^{-4} M phenol aqueous solution, separately. Before illumination, the suspension was placed in the dark under constant stirring for 90 min to reach adsorption / desorption equilibrium. Five millilitres of the suspension was taken out every 5 min for RhB and MO, every 10 min for phenol and centrifuged to remove the photocatalyst for UV-Vis absorption spectrum measurements. The concentration of RhB, MO and phenol was determined by monitoring their characteristic absorption at 553 nm, 462 nm and 270 nm, respectively. For the recycling experiments, first, 5 parallel experiments are performed; second, all the photocatalysts after the first cycle of photodegradation are collected, washed and dried; last, every 10 mg of treated photocatalysts was used to photodegrataion again. We repeated these processes of five times.

2.6 Photoelectrochemical Measurements:

The photoelectrodes were prepared according to literatures.[11,28-29] The indium doped oxide (ITO, Präzisions Glas & Optik GmbH, Germany) substrates were cleaned by ultrasonication in distilled water, ethanol, and isopropanol for 10 min sequentially. Both edges of the ITO substrates were covered with AB glue. Typically, the suspension was prepared by grinding 5 mg of the as-prepared products, 10 μL of PEDOT-PSS (Sigma-Aldrich, 1.3 wt%) aqueous solution and 50 μL of water, and the film was dried in air and annealed at 150 °C for 10 min. The photocurrents were measured by the Bio Logic potentiostats in a standard three-electrode system with the as-prepared samples as the working electrode, a Pt mesh as the counter electrode, and an Ag/AgCl electrode as a reference electrode. The solar simulator equipped a visible-light fibre-optical as light source. The 0.15 M KI/acetonitrile solution was used as the electrolyte.

3. Results and discussion

In this work, we prepared free-standing 2D square-like BiOI nanosheets via a very simple one-step solvothermal method. The crystallinity and phase purity of the as-prepared products were

confirmed by XRD analysis. As presented in Fig. 2, the XRD pattern could be well indexed to the tetragonal phase of BiOI with the lattice parameters of $a = b = 3.994$ Å and $c = 9.149$ Å, which is in good agreement with the standard card (JCPDF No. 10-0445). The strong and sharp peaks indicate that the as-prepared products are highly crystallized.

The morphological features of as-prepared 2D square-like BiOI nanosheets were characterized by SEM and TEM. The typical SEM and TEM images (as shown in Fig. 3a and 3c) are reveal that the as-prepared samples consist of large-scale nanosheet shaped structures with widths of about 100-300nm and thickness of around 10 nm. As shown in Fig. 3b and 3d, the SEM and TEM images of two individual nanosheets further confirmed the square-like shape of these nanosheets. The HRTEM (Fig. 3e) further indicated the highly crystalline nature of the nanosheets. The continuous clear lattice fringes with an interplanar lattice spacing of 0.282 nm and an angle of 90° correspond to the (110) atomic planes of the tetragonal BiOI. The spot SAED pattern (top right inset in Fig. 3e) revealed the single-crystalline characteristic of the square-like BiOI nanosheet. The angle of adjacent spots labeled in the SAED pattern is 45°, which is in agreement with the theoretical value of the angle between the (110) and (200) planes of tetragonal BiOI. It shows that

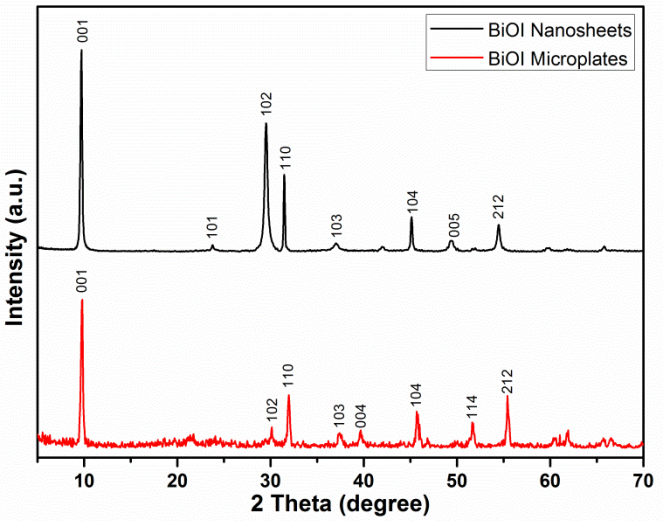

Fig. 2 XRD patterns of as-prepared 2D square-like BiOI nanosheets (Black) and BiOI microplate (red).

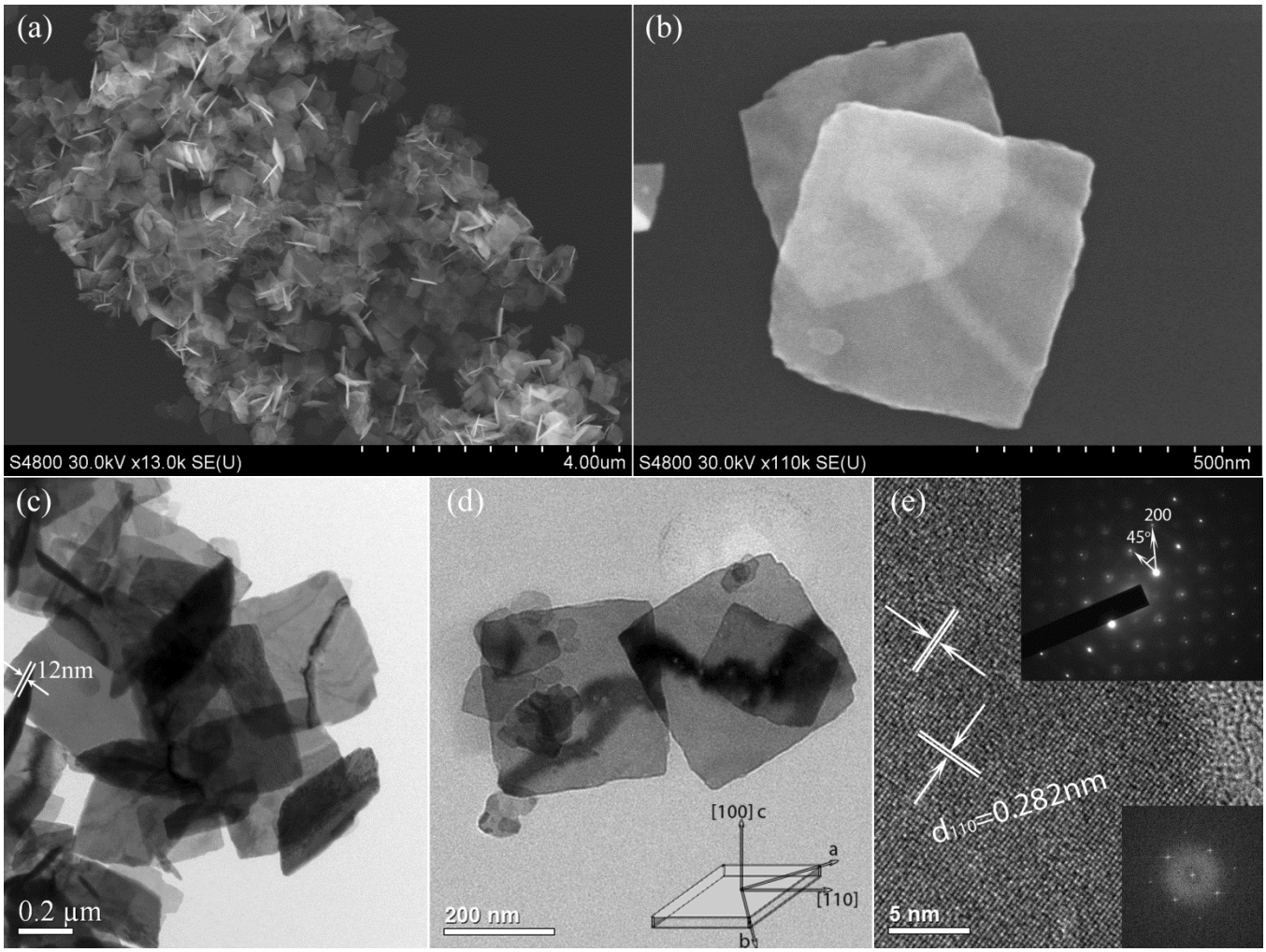

Fig. 3 (a) SEM image of large area of 2D square-like BiOI nanosheets; (b) the SEM image of two pieces 2D square-like BiOI nanosheets; (c) TEM image of bunches of 2D square-like BiOI nanosheets; (d) the TEM image of two pieces 2D square-like BiOI nanosheets and the schematic illustration of the crystal orientation of the BiOI nanosheet (inset bottom right); (e) the HRTEM image, SAED pattern (inset top right) and FFT pattern (inset bottom right) of 2D square-like BiOI nanosheet.

the set of diffraction spots can be indexed as the [001] zone axis, as shown in the inset of Fig. 3d. The fast fourier transform (FFT) image (bottom right inset in Fig. 3e) of the as-prepared square-like BiOI nanosheet shows the tetragonal structure, which agrees with the XRD result. Considering that the *c* parameter of BiOI is 9.149 Å, it can be inferred that each BiOI nanosheet consists of around 10 [I-Bi-O-Bi-I] units. As a comparison, BiOI microplate samples with micrometer-level side-width were also prepared.

The SEM image (Fig. 4) shows that these BiOI microplates are also square-like in morphology, with a size of 0.5-1.5 μm and thickness of more than 50 nm. The results of HRTEM and SAED of the as-prepared microplates are in accordance with those of the 2D square-like nanosheets. On the basis of the above structural information, the 2D square-like BiOI nanosheets have approximately of about 93% high reactive {001} facets exposed, whereas the BiOI microplates has a less precentage of around 85%. But at the same volume space, 2D square-like BiOI nanosheets have 3 more times of exposed {001} facets than BiOI microplates. This is proved by the BET results. As shown in Fig. 5, the specific surface area of the nanosheet BiOI is 38.32 $m^2 g^{-1}$, which is three more times than that of the microplate BiOI (11.10 $m^2 g^{-1}$).

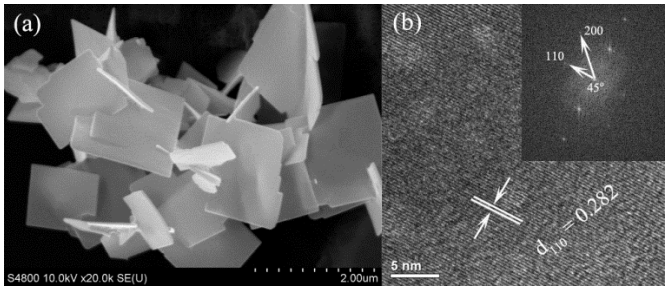

Fig. 4 (a) the SEM image of as-prepared BiOI microplates; (b) the HRTEM image and FFT pattern (inset) of as-prepared BiOI microplate

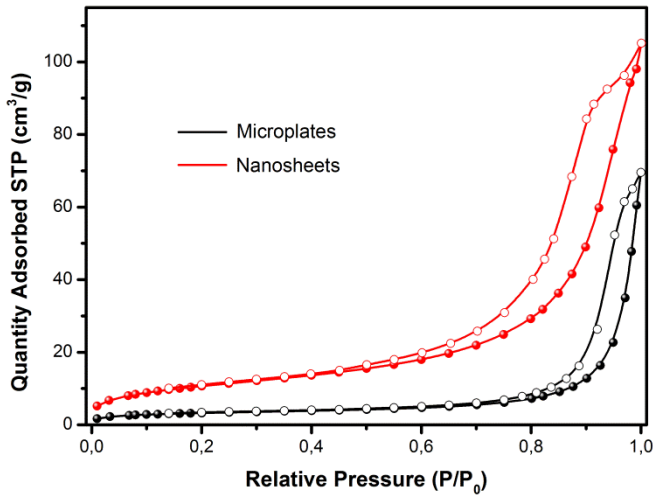

Fig. 5 Nitrogen adsorption / desorption isotherms of BiOI.

The energy band structure of a semiconductor is considered as a key factor to determinate its photocatalytic activity. Fig. 6 presents the UV-Vis absorption spectra of the 2D square-like BiOI nanosheets and BiOI microplates, in which a noticeable shoulder was observed at 730 nm and 653 nm, respectively. The bang gap value (Eg) could be evaluated by the equation of αhv = A (hv -Eg)n/2, where α, h, v, Eg and A are the absorption coefficient, Planck constant, light frequency, band gap energy, and a constant, respectively. Among them, n depends on the characteristics of the transition in a semiconductor. For BiOI, the value of n is 4 for the indirect transition. The band gap value of BiOI can be estimated by the curve of (αhλ)1/2 versus photon energy (hv) plotted. According to these, the band gap values of BiOI nanosheets is around 1.70 eV, slightly smaller than that of BiOI microplates (1.90 eV).

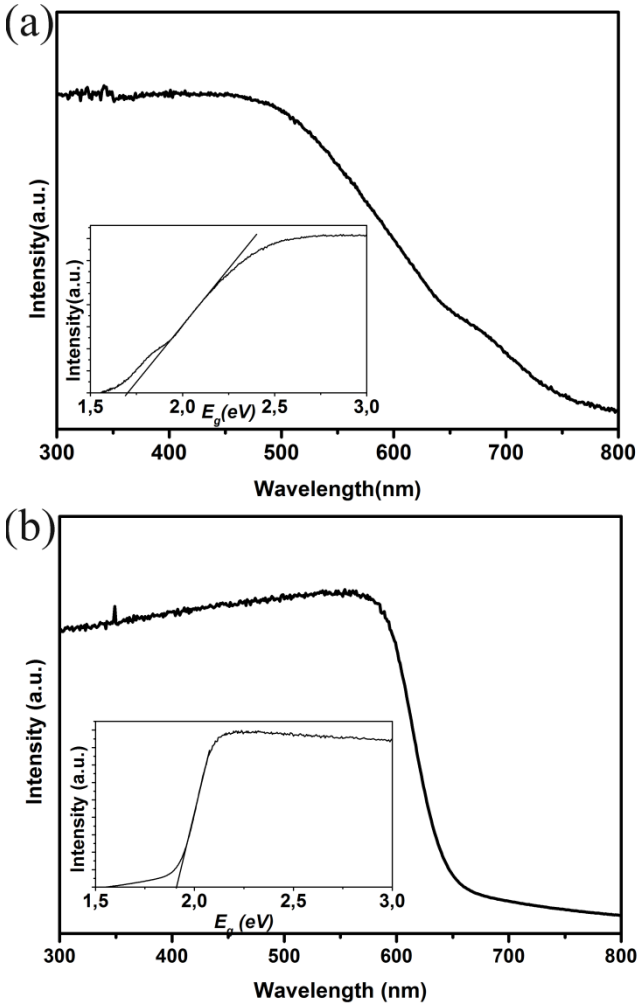

Fig. 6 UV-vis absorption spectra of as-prepared samples and their band gap values reckon by the curve of $(\alpha h\lambda)^{1/2}$ versus photon energy plotted. (a) 2D square-like BiOI nanosheets; (b) BiOI microplates.

The commonly used approach to characterize the activity of photocatalysts is to investigate the photocatalytic degradation of organic dyes or toxic pollutants, which is of great significance in environmental pollutant treatment. In our work, the photocatalytic performance of the 2D square-like BiOI nanosheets is evaluated under simulated solar irradiation with a 420 nm cut-off filter using RhB as a probe molecule in aqueous solution. The relevant data for the BiOI microplate is also given for comparison. As shown in Fig. 7a, the characteristic absorbance at 553 nm of RhB in aqueous solution decrease very fast with time of visible-light irradiation for 2D BiOI nanosheets. In contrast, the characteristic absorbance of BiOI microplates decrease much more slow under the same condition (Fig. 7b). As presented in Fig. 7c, in the absence of photocatalysts and under black condition with photocatalysts,

decomposition of RhB is inappreciable, suggesting that the photolysis of RhB is negligible within the test period. The decolouration rate of RhB in the presence of 2D square-like BiOI nanosheets reaches 90% after 15 min visible-light irradiation, but only around 25% of RhB molecules are decomposed within the same time. In order to clarify the stability of the high photocatalytic performance of the as-prepared 2D square-like BiOI nanosheets, recycling experiment for the photodegradation of RhB under visible-light irradiation was performed. As shown in Fig. 7d, the photodegradation rate remains constant over six more cycles; such excellent recyclability indicates the 2D square-like BiOI nanosheets is stable under visible-light irradiation, which is very important for its industrial application.

MO is an acid-base model organic pollutant and its color is determined by the azo bonds and their associated chromophores and auxochromes. The photocatalytic activity of 2D square-like BiOI nanosheets under visible light irradiation is further authenticated by photodegradation of MO in water, the relevant data for the BiOI microplate is also given for comparison. As shown in Fig. 8a, the characteristic absorbance of MO in water at 462 nm diminishes gradually as the exposure time under visible-light irradiation for 2D square-like BiOI nanosheets increases, and the absorption peak completely disappears after 15 min. However, the characteristic absorbance of BiOI microplates decrease extreme slowly at the same condition (Fig. 8b). As exhibited in Fig. 8c, in the absence of photocatalysts and black condition with photocatalysts, the decomposition of MO is negligible, which means the photolysis of MO is insignificant during the test period. The decolouration rate of MO reaches up to 94% after 15 min visible-light irradiation in the presence of 2D square-like BiOI nanosheets. But for BiOI microplates, the decolouration rate is only less than 7% within the same time visible-light irradiation. The recycling experiment for the photodegradation of MO under visible-light irradiation verified the excellent recyclability of as-prepared 2D square-like BiOI nanosheets. Over five more cycles, the photodegradation rate has no distinct difference (Fig. 8d), suggesting the as-prepared 2D square-like BiOI nanosheets are stable for visible light photocatalysis.

The health threat of phenol and phenolic pollutants is well known, great attention has been paid on their degradation during the last decades. However, all of their compounds have benzene rings, which present a strong inhibitive function for biological degradation. Here we performed photocatalysis degradation process for phenol to investigate the photocatalytic performance of as-prepared products. As presented in Fig. 9a, along with the time prolonging, the characteristic absorbance of phenol in water at 270 nm decrease under visible-light irradiation in the presence of 2D square-like BiOI nanosheets, and the degradation rate of phenol in water runs up to 70% after 60 min visible-light irradiation. With the same condition, the

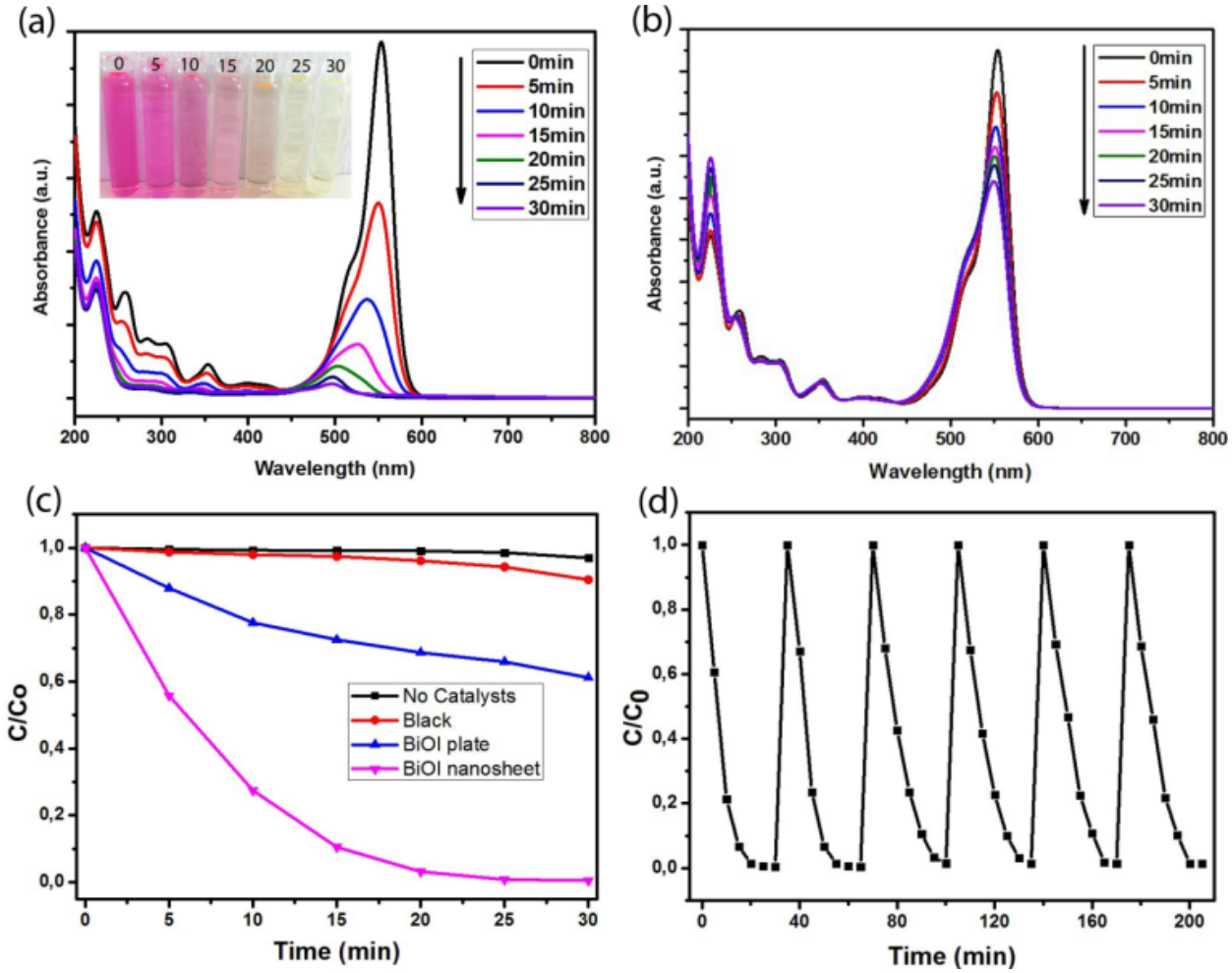

Fig. 7 Photocatalytic performance of the as-prepared 2D square-like BiOI nanosheets and BiOI microplates. (a) Visible light driven photodegradation of RhB with 2D square-like BiOI nanosheets; (b) Visible light driven photodegradation of RhB with BiOI microplates; (c) Comparison of decolouration efficiency under visible light irradiation; (d) Cycling curve of photodegradation of RhB with 2D square-like BiOI nanosheets.

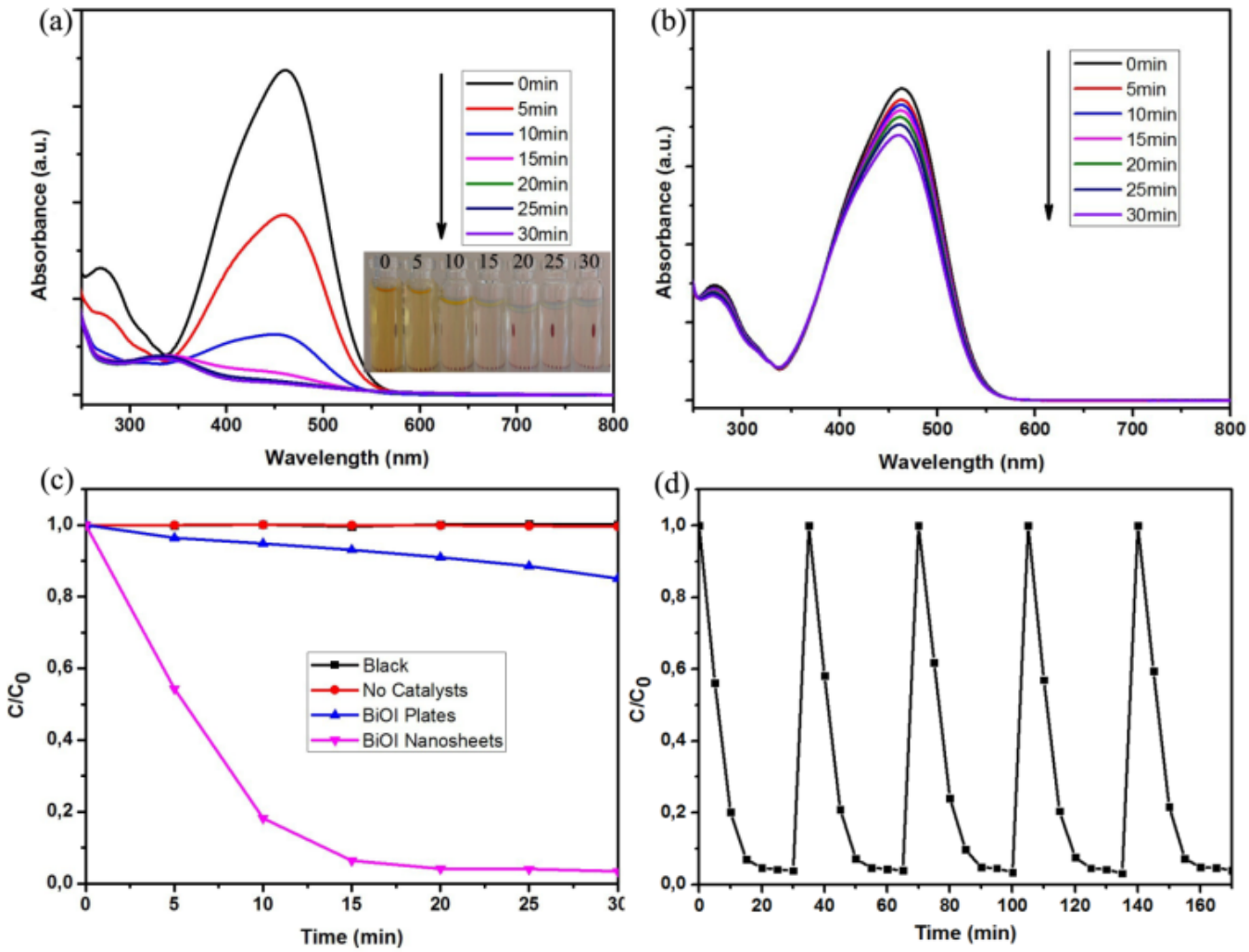

Fig. 8 Photocatalytic performance of the as-prepared 2D square-like BiOI nanosheets and BiOI microplates. (a) Visible light driven photodegradation of MO with 2D square-like BiOI nanosheets; (b) Visible light driven photodegradation of MO with BiOI microplates; (c) Comparison of discoloration efficiency under visible light irradiation; (d) Cycling curve of photodegradation of MO with 2D square-like BiOI nanosheets.

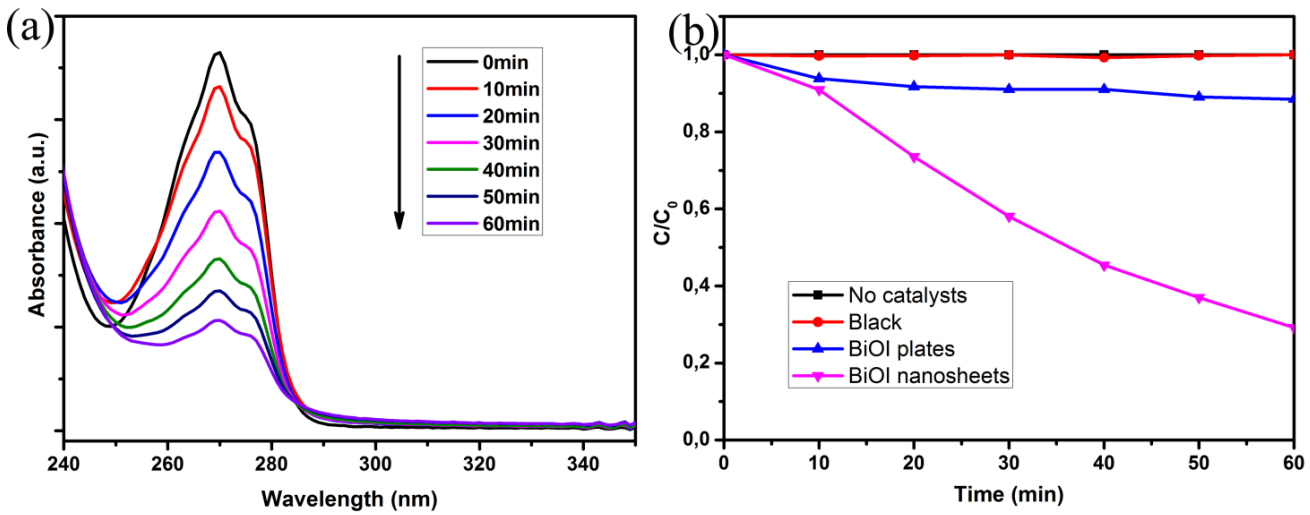

Fig. 9 (a) Photodegradation of phenol under visible light irradiation with 2D square-like BiOI nanosheets; and (b) Comparison of discoloration efficiency of 2D square-like BiOI nanosheets and BiOI microplates under visible light irradiation.

1111111111111111111111111111111111111111111111111111

contrastive BiOI microplates only have around 9% lessened. As a comparison, direct photolysis of phenol and 2D square-like BiOI nanosheets were carried out in the absence of photocatalysts and black condition with photocatalysts, respectively. The result exhibition in Fig. 9b is clarified that the direct photolysis of phenol and 2D square-like BiOI nanosheets are inappreciable.

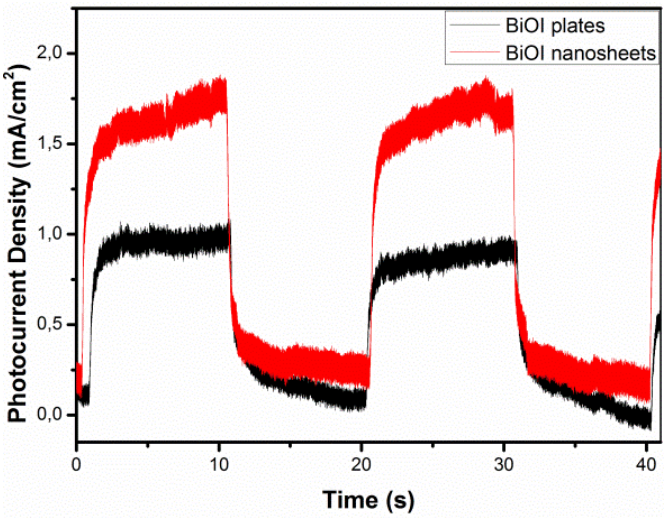

Fig. 10 Photocurrent responses of the 2D square-like BiOI nanosheets (red) and BiOI microplates (black) in 0.15 M KI/acetonitrile solution under visible light irradiation.

It is well-known that the photocatalytic degradation of dyes on semiconductors originates from two kinds of pathways, namely, they are direct semiconductor photoexcitation process and indirect dye self-photosensitization. In the RhB and MO photodegradation process, the characteristic absorbance peaks of RhB and MO are located at 553 nm and 462 nm, respectively. Both of them are in the visible-light region. Meanwhile, the photocatalyst has a narrow band gap, thus the two photocatalytic pathways could proceed. However, in the process of phenol photodegradation, the characteristic absorbance peak of phenol only locates at 270 nm and not in the visible-light region. Therefore, the degradation of phenol may mainly proceed in a direct semiconductor photoexcitation pathway under visible-light irradiation. Comparing with BiOI microplates, as-prepared 2D square-like BiOI nanosheets have smaller band gap, corresponding to higher utilization of solar light to generate more electron-hole pairs. On the basis of unique layered structure of the $[Bi_2O_2]$ slabs interleaved with double slabs of halogen atoms, it is could induce the presence of internal static electric fields that are perpendicular to the $[Bi_2O_2]$ slabs and halogen anionic slabs in BiOI. These induced internal static electric fields can improve the separation efficiency of the photoinduced electron-hole pairs. The BiOI nanosheets have more percentage of exposed {001} facets, which could induce the generation of stronger internal static electric fields.[30] Furthermore, the thin 2D BiOI nanosheets have a comparable more short distance for photoinduced electron-hole pairs to be effectively separated. In addition, the square-shaped structures have many uncoordinated surface atoms on the thin BiOI nanosheets, which further promote theirs photocatalytic activity. As confirmed by the transient photocurrent responses of the 2D BiOI nanosheets and BiOI microplates under visible light irradiation (Fig. 10), both electrodes generated photocurrents with a reproducible response to on/off cycles, but the BiOI nanosheets presented a higher photocurrent than that of the BiOI microplates, proving the more efficient photoinduced charge separation and transfer of BiOI nanosheets. Accordingly, 2D square-like BiOI nanosheets present higher photocatalytic activity than that of BiOI microplates under visible-light driven.

4. Conclusion

In summary, 2D square-like BiOI nanosheets have been synthesized via a low-cost and general hydrothermal process in the absence of surfactant and special solvent. The resulting BiOI nanosheets with the thickness of ~ 10 nm and the exposure of {001} facet exhibited high efficient photocatalytic activity by visible-light driven. Based on the photodegradation of phenol under visible-light, we proposed that the direct semiconductor photoexcitation pathway is dominant during the photocatalysis process. The efficient visible-light driven photocatalytic activity could be ascribed to the high percentage of exposed {001} facets and the thin 2D-square-shaped nanosheet. The high area of {001} facets are corresponding to efficient photogeneration electron-hole pairs separation, those based on the appropriate self-induced internal static electric fields of BiOI. And the thin nanosheets, further increased the separation efficiency of photoinduced electron-hole pairs. The as-prepared efficient 2D square-like BiOI nanosheets photocatalysts have the potential of industrial application. And the cost-effective fabrication process of 2D BiOI nanosheets could be a general method for achieving other BiOX 2D nanostructures in realizing high-performance photocatalysts.

Acknowledgements

This work was financially supported by European Research Council Grant and BMBF (3DNanoDevice). The authors appreciate the helps from Dr. Thomas Kups and Prof. Peter Schaaf for the TEM measurement.

Notes and references

Institute for Physics & IMN MacroNano® (ZIK), Technical University of Ilmenau, Prof. Schmidt-Str. 26, 98693 Ilmenau, Germany, Fax: (+) 49 3677-693746, E-mail: yong.lei@tu-ilmenau.de

1 A. Fujishima and K. Honda, *Nature*, 1972, **238**, 37.
2 K. D. Giglio, D. B. Green and B. Hutchinson, *J. Chem. Educ.*, 1995, **72**, 352.
3 M. G. Walter, E. L. Warren, J. R. Mckone, S. W. Boettcher, Q. Mi, E. A. Santori and N. S. Lewis, *Chem. Rev.*, 2010, **110**, 6446.
4 A. Bergmann, I. Zaharieva, H. Dau and P. Strasser, *Energy. Environ. Sci.*, 2013, **6**, 2745.
5 A. Kudo and Y. Miseki, *Chem. Soc. Rev.*, 2009, **38**, 253.
6 X. Chen, S. Shen, L. Guo and S. S. Mao, *Chem. Rev.*, 2010, **110**, 6503.
7 M. T. Mayer, C. Du and D. Wang, *J. Am. Chem. Soc.*, 2012, **134**, 12406.
8 A. Fujishima, T. N. Rao and D. A. Tryk, *J. Photoch. Photobio. C.*, 2000, **1**, 1.
9 J. S. Lee, K. H. You and C. B. Park, *Adv. Mater.*, 2012, **24**, 1084.
10 X. Chen, L. Liu, P. Y. Yu and S. S. Mao, *Science*, 2011, **331**, 746.

11 J. Jiang, K. Zhao, X. Xiao and L. Zhang, *J. Am. Chem. Soc.*, 2012, **134**, 4473.
12 M. Guan, C. Xiao, J. Zhang, S. Fan, R. An, Q. Cheng, J. Xie, M. Zhou, B. Ye and Y. Xie, *J. Am. Chem. Soc.*, 2013, **135**, 10411.
13 X. Xiao, C. Liu, R. Hu, X. Zuo, J. Nan, L. Li and L. Wang, *J. Mater. Chem.*, 2012, **22**, 22840.
14 W. Zhang, Q. Zhang and F. Dong, *Ind. Eng. Chem. Res.*, 2013, **52**, 6740.
15 J. Cao, X. Li, H. Lin, S. Chen and X. Fu, *J. Hazard. Mater.*, 2012, **239-240**, 316.
16 K. Zhao, L. Zhang, J. Wang, Q. Li, W. He and J. J. Yin, *J. Am. Chem. Soc.*, 2013, **135**, 15750.
17 K. Zhang, D. Zhang, J. Liu, K. Ren, H. Luo, Y. Peng, G. Li and X. Yu, *CrystEngComm*, 2012, **14**, 700.
18 X. Tu, S. Luo, G. Chen and J. Li, *Chem. Eur. J.*, 2012, **18**, 14359.
19 Y. Mi., Z. Huang, F. Hu, Y. Li and J. Jiang, *J. Phys. Chem. C*, 2009, **113**, 20795.
20 J. Feng, X. Sun, C. Wu, L. Peng, C. Lin, S. Hu, J. Yang and Y. Xie, *J. Am. Chem. Soc.*, 2011, **133**, 17832.
21 Y. Sun, Z. Sun, S. Gao, H. Cheng, Q. Liu, J. Piao, T. Yao, C. Wu, S. Hu, S. Wie and Y. Xie, *Nat. Commun.*, 2012, **3**, 1057.
22 R. Hao, X. Xiao, X. Zuo, J. Nan and W. Zhang, *J. Hazard. Mater.*, 2012, **209-210**, 137.
23 Y. Wang, K. Deng and L. Zhang, *J. Phys. Chem. C.*, 2011, **115**, 14300.
24 N. T. Hahn, S. Hoang, J. L. Self and C. B. Mullins, *ACS Nano*, 2012, **6**, 7712.
25 Y. Lei, G. Wang, S. Song, W. Fan, M. Peng, J. Tang and H. Zhang, *Dalton Trans.*, 2010, **39**, 3273.
26 K. Ren, K. Zhang, J. Liu, H. Luo, Y. Huang and X. Yu, *CrystEngComm*, 2012, **14**, 4384.
27 X. Xiao and W. D. Zhang, *J. Mater. Chem.*, 2010, **20**, 5866.
28 Y. J. Zhang, T. Mori, J. H. Ye and M. J. Antonietti, *J. Am. Chem. Soc.*, 2010, **132**, 6294.
29 G. H. Dong and L. Z. Zhang, *Mater. Chem.*, 2012, **22**, 1160.
30 J. Li, L. Z. Zhang, Y. J. Li and Y. Yu, *Nanoscale*, 2014, **6**, 167.

Table of Contents

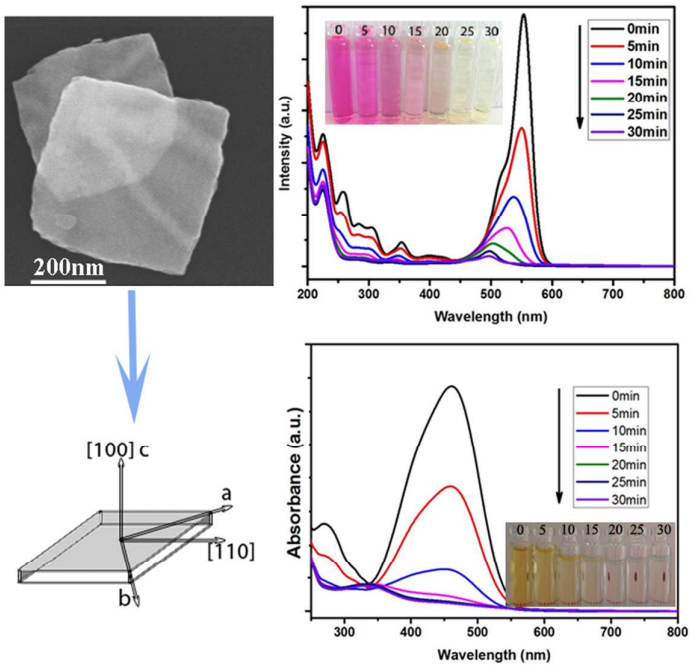

2D square-like BiOI thin nanosheets with exposure of {001} facets present high efficient visible-light photocatalytic performance.